EFFECTS OF NUCLEAR SPIN POLARIZATION ON REACTION DYNAMICS IN PHOTOSYNTHETIC BACTERIAL REACTION CENTERS

RICHARD A. GOLDSTEIN AND STEVEN G. BOXER
Department of Chemistry, Stanford University, Stanford, California 94305

ABSTRACT Singlet–triplet mixing in the initial radical-pair state, $P^{+}I^{-}$, of photosynthetic bacterial reaction centers is due to the hyperfine mechanism at low magnetic fields and both the hyperfine and Δg mechanisms at high magnetic fields (>1 kG). Since the hyperfine field felt by the electron spins in $P^{+}I^{-}$ is dependent upon the nuclear spin state in each radical, the relative probabilities of charge recombination to the triplet state of the primary electron donor, ^{3}PI, or the ground state, PI, will depend on the nuclear spin configuration. As a result these recombination products will have non-equilibrium distributions of nuclear spin states (nuclear spin polarization). This polarization will persist until the ^{3}PI state decays. In addition, due to unequal nuclear spin relaxation rates in the diamagnetic PI and paramagnetic ^{3}PI states, net polarization of the nuclear spins can result, especially in experiments that involve recycling of the system through the radical-pair state. This net polarization can persist for very long times, especially at low temperatures. Nuclear spin polarization can have consequences on any subsequent process that involves re-formation of the radical-pair state.

Numerical calculations of the nuclear polarization caused by both of these mechanics are presented, including the effect of such polarization on subsequent yields of ^{3}PI, ^{3}PI decay rates, the decay rate of the radical pair, and saturation behavior. The effect of this polarization under certain circumstances can be very dramatic and can explain previously noted discrepancies between experiments and theories that do not include nuclear spin polarization effects. Our analysis suggests new classes of experiments and indicates the need to reinterpret some past experimental results.

INTRODUCTION

In this paper we present numerical calculations of the effects of nuclear spin polarization on the initial reactions of photosynthetic reaction centers (RCs). Nuclear polarization effects have not been previously considered in analyses of RC reaction dynamics, but we find that they may play a significant role in determining the outcome of experiments under certain circumstances. Our analysis suggests several new types of experiments and indicates that the interpretation of certain standard experiments may require revision.

In *Rps. sphaeroides* RCs, absorption of light results in excitation of the special pair bacteriochlorophyll electron donor, P. The excited singlet state of P, *P, donates an electron to the initial electron acceptor, I, likely a bacteriopheophytin monomer, in ~2.8 ps (Martin et al., 1986), to form $P^{+}I^{-}$. $P^{+}I^{-}$ decays by electron transfer from I^{-} to a ubiquinone in ~200 ps (Rockley et al., 1975; Kaufmann et al., 1975). To study $P^{+}I^{-}$ it is useful to block this latter reaction, either by removal or prior reduction of the quinone. Under these conditions, $P^{+}I^{-}$ lives for ~10–20 ns before charge recombination occurs (Shuvalov and Parson, 1981). This is enough time for electron spin evolution between the nearly degenerate singlet and triplet electron spin states of the radical pair. Magnetic interactions such as nuclear hyperfine and electronic Zeeman interactions can affect this electron spin evolution and cause measurable effects due to the presence of reaction pathways that depend upon the electron spin state. The radical-pair mechanism (RPM) theory, originally developed to explain the nuclear spin polarization found in products of radical-pair reactions as detected by NMR spectroscopy (chemically induced dynamic nuclear polarization [CIDNP]) (Kaptein and Oosterhoff, 1969; Closs, 1969), was adapted (Werner et al., 1978; Haberkorn and Michel-Beyerle, 1979) to the RC problem. This theory has been very successful in analyzing the spin dynamics of blocked RCs, including explaining the effects of external magnetic fields on experimental observables (for a recent review, see Hoff, 1986).

One of the predictions of the RPM theory is that nuclear polarization may occur under certain circumstances. Nuclear spin polarization arises because the nuclear hyperfine interaction plays a key role in determining the spin dynamics of the radical-pair state. Because the relative probabilities of a particular RC forming various product states depend upon the nuclear spin state of that RC, different product states will be enriched with particular nuclear spin configurations. The effects of this enrichment

are manifested during subsequent re-formation of the radical-pair state, either by intrinsic reaction pathways or by reexcitation of spin-polarized products.

A preliminary account of these results has been presented previously (Goldstein and Boxer, 1986).

REACTION SCHEME

Fig. 1 *A* shows the basic reaction scheme used to analyze the kinetics of quinone-depleted *Rps. sphaeroides* R-26 RCs. Photoexcitation of the electron donor forms *P, which transfers an electron to I to form the singlet-correlated radical-ion pair $^1(P^+I^-)$ with rate k_1. The rate of *P fluorescence is small relative to k_1 and is neglected in these calculations. A detailed analysis of the effects of spin dynamics on *P fluorescence will be presented in a subsequent paper (Goldstein, R. A., and S. G. Boxer, work in progress). The singlet-correlated radical pair either reforms *P (rate k_{-1}), recombines to the ground state, PI (rate k_S), or undergoes coherent spin evolution at frequency ω to form the triplet radical-pair state, $^3(P^+I^-)$. This triplet radical pair state either re-evolves to form the singlet radical-pair state or recombines to form the triplet state of the electron donor and the ground state of I, ^{3}PI (rate k_T). ^{3}PI either decays to the ground state by intersystem crossing (rate k_{isc}) or thermally repopulates the triplet radical-pair state (rate k_b). The latter pathway was introduced by us in an earlier paper to explain the temperature and magnetic field–dependent rate of ^{3}PI decay (k_{obs}) (Chidsey et al., 1985). Assuming fast electron and nuclear spin relaxation in ^{3}PI relative to k_{obs} (i.e., equilibrium spin distribution in the ^{3}PI state at all times during its decay), we showed that k_{obs} is given by

$$k_{obs} = k_{isc} + \tfrac{1}{3}\Phi_{^3PI}k_b, \qquad (1)$$

where $\Phi_{^3PI}$ is the total initial ^{3}PI quantum yield and k_b is equal to $k_T \exp(-\Delta H/kT)$, where ΔH is the enthalpy difference between the ^{3}PI and radical pair state, k is the Boltzmann constant, and T is the temperature. Most of the decay of ^{3}PI at room temperature proceeds via this second passage through the singlet–triplet mixing process. It was the analysis of this process and the question of whether singlet–triplet mixing in the radical pairs re-formed from ^{3}PI was the same as for those formed from *PI that led us to consider nuclear spin polarization (Chidsey et al., 1985).

A

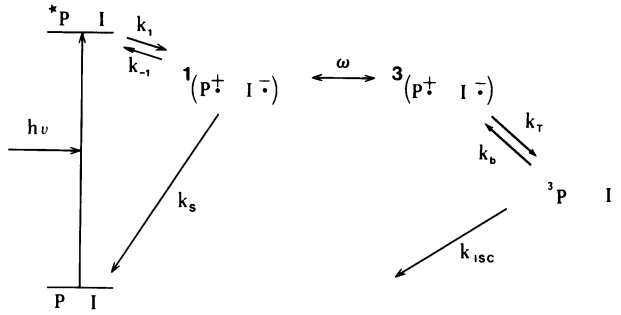

B

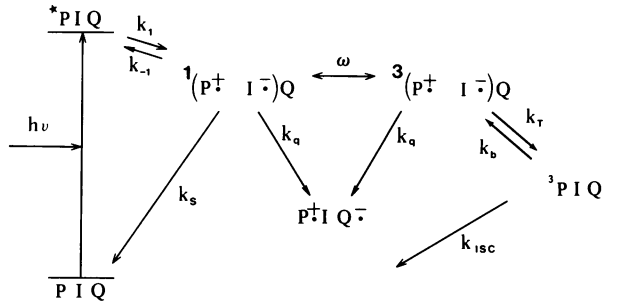

FIGURE 1 (*A*) Kinetic scheme for the initial photochemistry of RCs when electron transfer from the initial electron acceptor, I, to the quinone, Q, has been blocked. P is the initial electron donor. (*B*) Kinetic scheme including the quinone-reduction pathway.

METHODOLOGY

We use the semiclassical approach of Schulten and Wolynes to model the electron spin evolution (Schulten and Wolynes, 1978). In this model, mixing between the singlet and triplet radical-pair states occurs as the spins of the two unpaired electrons in the radical pair precess independently around different magnetic fields, each equal to the sum of the applied magnetic field and the hyperfine field of that molecule. The nuclear spin state does not change. Since there are a large number of nuclear spins, there is a distribution of nuclear spin states, and the sample is intrinsically heterogeneous with respect to hyperfine fields.

The total hyperfine field is modeled as the end-to-end distance of a freely jointed polymer chain, with each link representing the hyperfine field of an individual nuclear spin (Schulten and Wolynes, 1978). At zero external field, it is the total magnitude of the difference in hyperfine fields felt by the two electrons that determines the singlet–triplet mixing frequency ω:

$$\omega = g\beta\frac{|\mathbf{H}_1 - \mathbf{H}_2|}{\hbar} \quad \text{(zero external field)}, \qquad (2)$$

where g is the electron g value, β is the Bohr magneton, and $\mathbf{H}_i$ is the hyperfine field for electron i. The sum of the hyperfine fields influences the singlet–triplet mixing by splitting the singlet and triplet energy levels and causing spin evolution within the triplet manifold. Assuming a large number of nuclei with similar hyperfine coupling

constants, the equilibrium distribution of hyperfine fields, $R^0(\mathbf{H}_1, \mathbf{H}_2)$, at zero external field is:

$$R^0(\mathbf{H}_1, \mathbf{H}_2) = \frac{1}{2\pi A_1 A_2} \exp\left\{-\frac{1}{2}\left(\frac{H_1^2}{A_1^2} + \frac{H_2^2}{A_2^2}\right)\right\} \quad \text{(zero external field)}, \quad (3)$$

where A_i represents the width of the hyperfine field distribution for electron i. $R^0(\mathbf{H}_1, \mathbf{H}_2)$ can be expressed in terms of ω, and Eq. 3 can then be integrated over the other variables to give the equilibrium distribution of ω values, $R^0(\omega)$:

$$R^0(\omega) = \frac{\omega^2}{(2\pi)^{1/2}\alpha^3} \exp\left\{-\frac{1}{2}\left(\frac{\omega^2}{\alpha^2}\right)\right\} \quad \text{(zero external field)}, \quad (4)$$

where

$$\alpha = g\beta \frac{(A_1^2 + A_2^2)^{1/2}}{\hbar}. \quad (5)$$

The spherical-Gaussian nature of Eq. 4 reflects the fact that $\mathbf{H}_1$-$\mathbf{H}_2$ can point in any direction in space. Whereas Eq. 2 implies that ω is always positive, only the absolute value of ω has physical significance, so $R^0(\omega)$ is considered to extend from $-\infty$ to $+\infty$ to be consistent with the high field formulation that follows.

For large external fields (>1 kG), the electron Zeeman interaction inhibits electron spin evolution to any other triplet sublevel besides the T_0 state, so only the $\hat{\mathbf{z}}$ components of the hyperfine fields contribute to singlet–triplet mixing. In addition, there is a contribution to ω reflecting the difference in precession frequencies for the two electrons around the externally applied field, $\mathbf{B}_{ext}$ (Δg effect). The sum of the hyperfine fields can now be neglected because triplet sublevel mixing is inhibited by the large Zeeman splitting between triplet sublevels, and the hyperfine field does not cause Zeeman splitting of the S and T_0 states. The result is a Gaussian distribution for $R^0(\omega)$ centered at $\omega_0 = \Delta g\beta|\mathbf{B}_{ext}|/\hbar$, where Δg is the difference in g-values for the two unpaired electrons

$$R^0(\omega) = \frac{1}{(2\pi)^{1/2}\alpha} \exp -\frac{1}{2}\left(\frac{(\omega - \omega_0)^2}{\alpha^2}\right) \quad \text{(high external field)}. \quad (6)$$

This distribution is related to the well-known lineshape in electron paramagnetic resonance (EPR) spectroscopy when there is unresolved hyperfine splitting, as is the case in RCs (Hoff, 1979). Because the difference in electron spin precession rates around $\mathbf{B}_{ext}$ can be either positive or negative, the sign of ω is physically significant, and $R^0(\omega)$ can extend from $-\infty$ to $+\infty$.

The distributions of hyperfine fields given in Eqs. 4 and 6 reflect the nuclear spin state and are considered independent of the electronic state of P and I. In particular, the equilibrium distribution, $R^0(\mathbf{H}_i)$, is the same in the PI, ^{3}PI, and P^+I^- states. The energy gap between singlet and triplet radical-pair states is set equal to 2J at all fields. The electron–dipole electron–dipole interaction is neglected, as are all other anisotropic interactions. While some analyses include a large dipole interaction (Roelofs et al., 1982; Norris et al., 1982), the distance between likely locations of P^+ and I^- in the *Rp. viridis* RC as measured by x-ray diffraction (Deisenhofer et al., 1984) suggests that this may not be physically reasonable (Ogrodnik et al., 1985). The isotropic part of A_i can be obtained from EPR and electron-nuclear double resonance measurements of P^+ and I^- (Hoff, 1979). All reaction paths besides ω are considered independent of external magnetic field and nuclear spin state.

The stochastic Liouville equation is used to model the time evolution of the radical-pair state. For RCs with particular values of $\mathbf{H}_i$, the time evolution of $\rho(\mathbf{H}_i, t)$, the density matrix describing the radical-pair state, is given by

$$\frac{d}{dt}\rho(\mathbf{H}_i, t) = -\frac{i}{\hbar}\{\mathcal{H}(\mathbf{H}_i), \rho(\mathbf{H}_i, t)\}_- - \frac{1}{2}(k_S + k_{-1})\{\hat{\mathbf{P}}^S, \rho(\mathbf{H}_i, t)\}_+ - \frac{1}{2}k_T\{\hat{\mathbf{P}}^T, \rho(\mathbf{H}_i, t)\}_+ + \frac{k_1[{}^*\mathrm{PI}(\mathbf{H}_i, t)]}{\mathrm{Tr}\,\hat{\mathbf{P}}^S}\hat{\mathbf{P}}^S, \quad (7)$$

where $\mathcal{H}(\mathbf{H}_i)$ is the spin Hamiltonian for RCs with hyperfine fields $\mathbf{H}_i$, $\hat{\mathbf{P}}^S$ and $\hat{\mathbf{P}}^T$ are the singlet and triplet spin projection operators, respectively, $[{}^*\mathrm{PI}(\mathbf{H}_i)]$ is the relative concentration of *PI with those particular values of $\mathbf{H}_i$, $\{A, B\}_-$ and $\{A, B\}_+$ represent the commutator and anticommutator of operators A and B, respectively, and Tr represents trace. The time evolution of $[{}^*\mathrm{PI}(\mathbf{H}_i)]$ is given by

$$\frac{d}{dt}[{}^*\mathrm{PI}(\mathbf{H}_i, t)] = k_{-1}\mathrm{Tr}(\hat{\mathbf{P}}^S\rho(\mathbf{H}_i, t)) - k_1[{}^*\mathrm{PI}(\mathbf{H}_i, t)]. \quad (8)$$

The triplet yield for RCs with hyperfine fields $\mathbf{H}_i$, $\phi(\mathbf{H}_i)$, is then

$$\phi(\mathbf{H}_i) = k_T\mathrm{Tr}(\hat{\mathbf{P}}^T\bar{\rho}(\mathbf{H}_i)) \quad (9)$$

where

$$\bar{\rho}(\mathbf{H}_i) = \int_0^\infty \rho(\mathbf{H}_i, t)\, dt. \quad (10)$$

Following other analyses (Werner et al., 1978), we use the steady-state approximation for $[{}^*\mathrm{PI}(\mathbf{H}_i)]$ (valid after its initial decay) and integrate Eq. 7 subject to the initial condition

$$\rho(\mathbf{H}_i, 0) = \frac{\hat{\mathbf{P}}^S}{\mathrm{Tr}\,\hat{\mathbf{P}}^S} \quad (11)$$

to obtain

$$\frac{\hat{\mathbf{P}}^S}{\mathrm{Tr}\,\hat{\mathbf{P}}^S} = \frac{i}{\hbar}\{\mathcal{H}(\mathbf{H}_i), \bar{\rho}(\mathbf{H}_i)\}_- + \frac{1}{2}(k_S + k_{-1})\{\hat{\mathbf{P}}^S, \bar{\rho}(\mathbf{H}_i)\}_+ + \frac{1}{2}k_T\{\hat{\mathbf{P}}^T, \bar{\rho}(\mathbf{H}_i)\}_+ - \frac{k_{-1}\mathrm{Tr}(\hat{\mathbf{P}}^S\bar{\rho}(\mathbf{H}_i))}{\mathrm{Tr}\,\hat{\mathbf{P}}^S}\hat{\mathbf{P}}^S. \quad (12)$$

For high external fields (>1 kG), in the reduced basis set $\{S, T_0\}$, $\mathcal{H}(\mathbf{H}_i)$ is

$$\mathcal{H}(\mathbf{H}_i) = \begin{bmatrix} J & \frac{\omega}{2} \\ \frac{\omega}{2} & -J \end{bmatrix} \quad \text{(high external field)}. \quad (13)$$

In this case, the solution of Eq. 12 is straightforward:

$$\phi(\mathbf{H}_i) = \frac{k_T}{k_S + k_T}\left[\frac{\omega^2}{\omega^2 + \kappa^2}\right] \quad \text{(high external field)}, \quad (14)$$

where

$$\kappa^2 = \frac{k_S k_T (k_S + k_T + k_{-1})}{k_S + k_T} + \frac{16J^2(k_S k_T)}{(k_S + k_T + k_{-1})(k_S + k_T)}. \quad (15)$$

In the zero field case, the basis set must include all of the triplet levels, and it is more practical to solve the full matrix equation for each particular set of values of $\mathbf{H}_i$ numerically.

The total ^{3}PI yield, when the ground state distribution of $\mathbf{H}_i$ is given by $R_{PI}(\mathbf{H}_i)$, is

$$\Phi_{^3PI} = \int_{-\infty}^{\infty} R_{PI}(\mathbf{H}_i)\phi(\mathbf{H}_i)\,d\mathbf{H}_i. \quad (16)$$

J and k_{-1} both affect $\phi(\mathbf{H}_i)$ and $\Phi_{^3PI}$ in similar ways, by interfering with the singlet–triplet mixing. This can be seen explicitly at high external magnetic fields, where both parameters only affect κ^2. Because of this, k_{-1} will not be explicitly included in the following calculations.

The presence of coherence in the spin evolution in the radical-pair state introduces nonexponential behavior to the decays. A characteristic decay rate is defined following Haberkorn and Michel-Beyerle (1979)

$$k_{decay} = \frac{C(0)}{\int_0^{\infty} C(t)\,dt}, \quad (17)$$

where $C(t)$ is the concentration of the decaying state as a function of time. This expression gives the standard decay rate in the case of exponential decays. Using this definition, they showed that the radial pair decay rate k_{RP}, is given by

$$k_{RP} = \left(\frac{(1 - \Phi_{^3PI})}{k_S} + \frac{\Phi_{^3PI}}{k_T}\right)^{-1}. \quad (18)$$

The observed triplet decay rate, k_{obs}, when nuclear spin relaxation in the ^{3}PI state is slow relative to k_{obs}, is then:

$$k_{obs} = \frac{\int_{-\infty}^{\infty} R_{^3PI}(\mathbf{H}_i)\,d\mathbf{H}_i}{\int_{-\infty}^{\infty} \frac{R_{^3PI}(\mathbf{H}_i)}{k_{dec}(\mathbf{H}_i)}\,d\mathbf{H}_i}, \quad (19)$$

where

$$k_{dec}(\mathbf{H}_i) = k_{isc} + \tfrac{1}{3}\phi(\mathbf{H}_i)k_b, \quad (20)$$

and $R_{^3PI}(\mathbf{H}_i)$ is the distribution of hyperfine fields in the ^{3}PI state. Eqs. 19 and 20 are the form of Eq. 1 modified to include nuclear polarization effects.

In the following sections we model the RC reaction dynamics using the parameter values shown in Table I. These are reasonable values for Q-depleted *Rps. sphaeroides* R26.1 RCs (Boxer et al., 1983; Hoff, 1986; Lersch and Michel-Beyerle, 1983; Norris et al., 1982). Moderate variations in the values of these parameters do not affect the qualitative features of this analysis.

NUCLEAR SPIN POLARIZATION PRODUCED BY SORTING IN THE RADICAL-PAIR STATE

The simplest example of a process that leads to nuclear spin polarization is spin sorting, which occurs during the initial decay of the radical pair to PI or ^{3}PI. After excitation and charge separation, those RCs with hyperfine fields that cause rapid singlet–triplet mixing in the radical-pair state will form ^{3}PI more readily than those with hyperfine fields corresponding to slow singlet–triplet mixing. As a result, RCs in the ^{3}PI state will be enriched in these particular nuclear spin states. After a delta-function saturating flash of light, the distributions of $\mathbf{H}_i$ values in the ^{3}PI and re-formed ground states, $R_{^3PI}(\mathbf{H}_i)$ and $R_{PI}(\mathbf{H}_i)$,

TABLE I
VALUES OF KINETIC AND MAGNETIC PARAMETERS USED TO CREATE THEORETICAL CURVES IN FIGS. 2–7

Parameter	Value
k_S	$5.0 \times 10^7\ s^{-1}$
k_T	$5.0 \times 10^8\ s^{-1}$
k_{-1}	0.0*
k_{isc}	$1.0 \times 10^4\ s^{-1}$
A_P	9.5 G
A_I	13.0 G
J	7.0 G
Δg	0.001
T	300°K

*See comment after Eq. 16.

respectively, will be given by

$$R_{^3PI}(\mathbf{H_i}) = \phi(\mathbf{H_i})R^0(\mathbf{H_i}) \quad (21)$$

and

$$R_{PI}(\mathbf{H_i}) = (1 - \phi(\mathbf{H_i}))R^0(\mathbf{H_i}). \quad (22)$$

The most dramatic manifestation of this resulting nuclear polarization will be in the polarization of the ω values in the RCs in the re-formed ground and ^{3}PI state. Specifically, RCs with large values of ω will be overrepresented in the ^{3}PI state, while RCs with smaller values of ω will preferentially re-form the ground state. Distributions of ω in ^{3}PI and PI can be obtained by expressing Eqs. 21 and 22 in terms of ω and integrating over the other parameters. Plots of $R_{^3PI}(\omega)$ and $R_{PI}(\omega)$ at various applied magnetic fields are presented in Fig. 2. For ease of comparison, these curves have been normalized so that the integrated areas are equal. Assuming slow nuclear spin relaxation in PI and ^{3}PI compared with k_{obs}, this nuclear polarization will last until the ^{3}PI state decays (~30–150 μs, depending on temperature).

This nuclear spin polarization can have observable effects in any subsequent process that depends upon the distribution of $\mathbf{H_i}$ values in either the PI or ^{3}PI states, processes that involve repassage of the RCs through the radical-pair state. For example, consider the decay path of ^{3}PI that proceeds by repopulation of $^3(P^+I^-)$, singlet–triplet mixing to $^1(P^+I^-)$, and decay to PI via k_S. The higher-than-equilibrium concentration of RCs in the ^{3}PI state with large ω values would facilitate ^{3}PI decay through this path and result in a faster observed rate of ^{3}PI decay than would be predicted for an equilibrium distribution of nuclear spins in this state. The calculated effect of this polarization on k_{obs} is shown in Fig. 3 *A*. This plot also illustrates a general characteristic of nuclear spin polarization effects—any effect of nuclear spin polarization becomes negligible at very high field as the spread in singlet–triplet mixing frequencies due to the distribution of nuclear spin states becomes small relative to the $\Delta g\beta|\mathbf{B_{ext}}|/\hbar$ contribution to singlet–triplet mixing.

The theoretical analysis of the magnetic field dependence of k_{obs} not including nuclear spin polarization effects led us to the prediction that k_{obs} and $\Phi_{^3PI}$ should increase in parallel as $\mathbf{B_{ext}}$ is increased (Eq. 1). However, we observed that the change in k_{obs} between 1 to 50 kG was less than that expected given the observed change in $\Phi_{^3PI}$ (Chidsey et al., 1985). As shown in Fig. 3, when nuclear polarization effects are included in the analysis, the predicted change in k_{obs} with $\mathbf{B_{ext}}$ is less than that predicted by Eq. 1, in agreement with the experimental observations. Nuclear spin polarization is the likely explanation for the discrepancy (Chidsey et al., 1985).

Another effect of nuclear spin polarization will be to change the results of a flash photolysis experiment performed by reexciting that fraction of RCs that re-form the ground state via k_s, before the ^{3}PI state has a chance to decay. Shown in Fig. 3 *B* and Fig. 3 *C* are the effects of this polarization on the second passage triplet yield and radical-pair decay rate (k_{RP}). The triplet yield for the second flash is lower, reflecting the bias of the re-formed ground state RCs due to the first flash towards smaller ω values, which cannot readily form ^{3}PI. Likewise, the radical pair decays at a slower rate after a second flash, as more of the RCs decay by the slower k_s path. These effects will complicate the analysis of experiments where the sample is excited at high repetition rates or where a strong flash of duration longer than ~2 ns is used, both common experimental conditions.

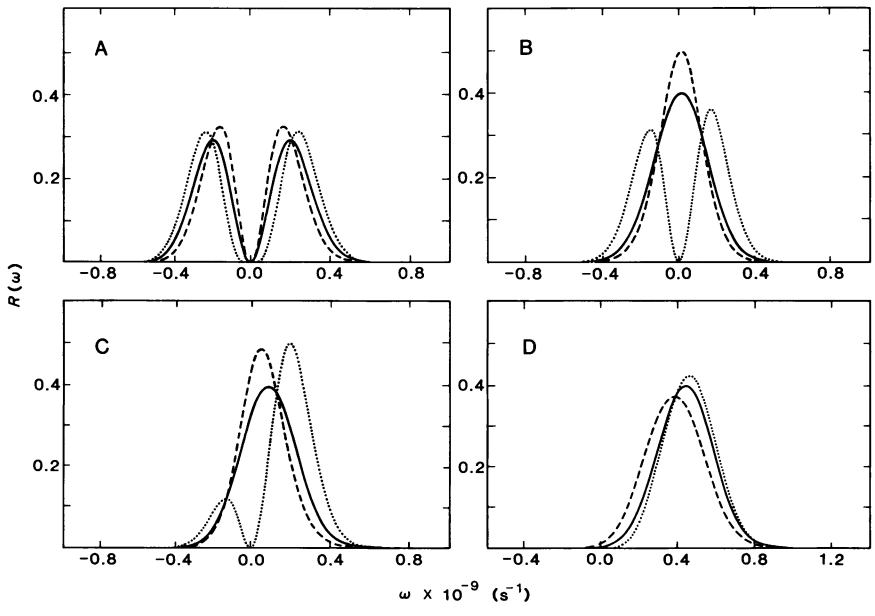

FIGURE 2 Distribution of ω values [$R(\omega)$] in the PI [$R_{PI}(\omega)$] (---) and ^{3}PI state [$R_{^3PI}(\omega)$] (· · ·) after saturating delta-function excitation, compared with the equilibrium distribution [$R^0(\omega)$] (——), at 0 G (*A*), 1 kG (*B*), 20 kG (*C*), and 50 kG (*D*). All distributions have been normalized so that the integrated areas are equal. Note the difference in abcissa scales.

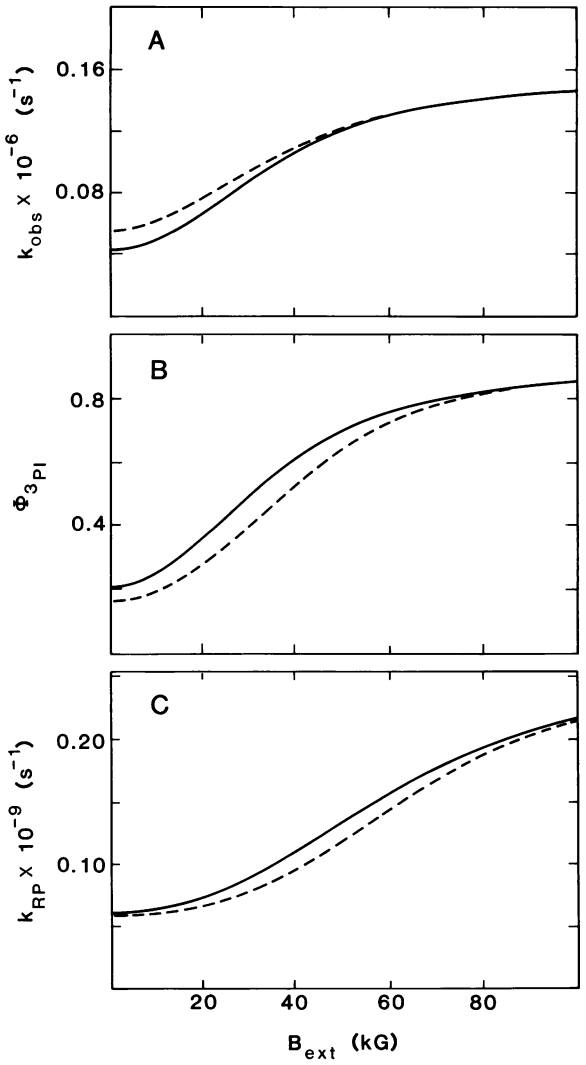

FIGURE 3 (*A*) The effect of the nuclear polarization produced by sorting in the radical-pair state on the observed ^{3}PI decay rate, k_{obs}, as a function of external magnetic field. Shown are predicted values of k_{obs} when the nuclear spins in the ^{3}PI state are at equilibrium at all times during the decay (Eq. 1) (—), and when the effects of nuclear polarization are included in the analysis (Eq. 19) (----). (*B* and *C*) The effect of this nuclear polarization on the yield of ^{3}PI (*B*) and k_{RP} (*C*) for a flash photolysis experiment performed on the re-formed ground state after an initial excitation, as a function of external magnetic field. Calculated values for a polarized sample (----) are compared with calculations for excitation of a sample at equilibrium, as for instance, the initial excitation (—).

COMPETITION WITH QUINONE REDUCTION

The model can be easily modified to include the presence of the next electron accepter in the electron transport chain. The reaction scheme is shown in Fig. 1 *B*. k_q is the rate of formation of P^+IQ^- from P^+I^-Q and is considered independent of the spin state of P^+I^-. k_q is too fast with native ubiquinone ($\sim 5 \times 10^{10}$ s^{-1} [Rockley et al., 1975; Kaufmann et al., 1975]) for appreciable electron spin evoluation to take place in P^+I^-Q before decay to P^+IQ^-, so no ^{3}PI formation or nuclear spin polarization would be expected. However, other quinones have been substituted for ubiquinone resulting in smaller values of k_q (Gunner et al., 1986; Okamura et al., 1975). k_q is also considerably smaller when the non-heme Fe(II) is removed (Kirmaier et al., 1986). In such cases, it is possible that singlet–triplet mixing can compete with k_q, and ^{3}PI can be formed, albeit in lower yield than for Q-depleted RCs.

The resulting reaction dynamics can be analyzed with a simple extension of the analysis given above. The distributions of $\mathbf{H}_i$ values in the ^{3}PI and ground state are then:

$$R_{^3PI}(\mathbf{H}_i) = \phi_{^3PI}(\mathbf{H}_i)R^0(\mathbf{H}_i) \quad (23)$$

$$R_{PI}(\mathbf{H}_i) = \phi_{PI}(\mathbf{H}_i)R^0(\mathbf{H}_i), \quad (24)$$

where the equations governing the radical pair evolution are:

$$\frac{\hat{\mathbf{P}}^S}{\mathrm{Tr}[\hat{\mathbf{P}}^S]} = \frac{i}{\hbar}\{\mathcal{H}(\mathbf{H}_i), \bar{\rho}(\mathbf{H}_i)\}_- + \frac{1}{2}(k_S + k_q)\{\hat{\mathbf{P}}^S, \bar{\rho}(\mathbf{H}_i)\}_+ + \frac{1}{2}(k_T + k_q)\{\hat{\mathbf{P}}^T, \bar{\rho}(\mathbf{H}_i)\}_+ \quad (25)$$

$$\phi_{^3PI}(\mathbf{H}_i) = k_T \mathrm{Tr}[\hat{\mathbf{P}}^T\bar{\rho}(\mathbf{H}_i)] \quad (26)$$

$$\phi_{PI}(\mathbf{H}_i) = k_S \mathrm{Tr}[\hat{\mathbf{P}}^S\bar{\rho}(\mathbf{H}_i)]. \quad (27)$$

If the nuclear spin states in the ^{3}PI state are considered to always be in equilibrium, k_{obs} is given by

$$k_{obs} = k_{isc} + \left[\frac{k_T k_q}{k_T + k_q} + \frac{1}{3}k_T\left(\frac{k_S + k_q}{k_T + k_q}\right)\Phi_{^3PI}\right]e^{-\Delta H/kT}. \quad (28)$$

This represents a simple extension of the theory we have presented earlier (Eq. 1) (Chidsey et al., 1985). To calculate k_{obs} for a nuclear spin polarized sample, $R_{^3PI}(\mathbf{H}_i)$ from Eq. 23 is substituted into Eq. 19 with

$$k_{dec}(\mathbf{H}_i) = k_{isc} + \left[\frac{k_T k_q}{k_T + k_q} + \frac{1}{3}k_T\left(\frac{k_S + k_q}{k_T + k_q}\right)\phi_{^3PI}(\mathbf{H}_i)\right]e^{-\Delta H/kT}. \quad (29)$$

Fig. 4 shows the dependence of k_{obs} on k_q, both with and without nuclear spin polarization effects. The effect of nuclear spin polarization on k_{obs} is insignificant as most of the decay of ^{3}PI goes through spin-independent k_q for any but small values for k_q. Note, however, that electron transfer from I^- to Q opens a new decay pathway (k_q) for ^{3}PI decay, which results in a dramatic change in k_{obs}: the triplet decay rate of quinone-substituted RCs is expected to be much faster than in Q-depleted RCs. Assuming that the scheme in Fig. 1 *B* is complete, any triplet state decaying with a lifetime of ~20–40 μs at room temperature in quinone-substituted RCs is likely from RCs which are

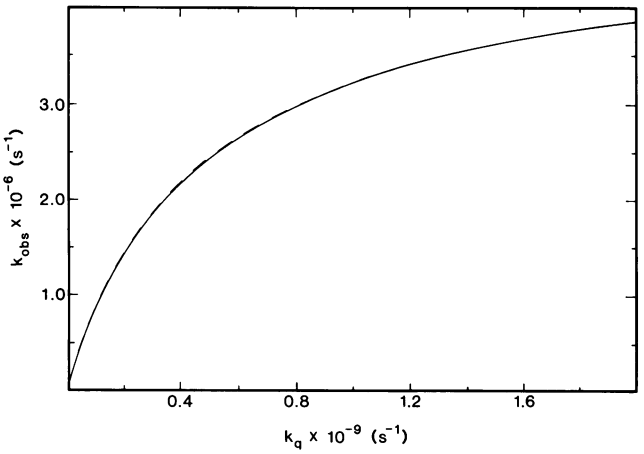

FIGURE 4 The effect of nuclear polarization on the ^{3}PI decay rate, k_{obs}, at 0 G when the quinone reduction pathway (k_q) is included in the analysis (Fig. 1 *B*). k_{obs} is shown as a function of k_q when the nuclei in the ^{3}PI state are at equilibrium at all times during the decay (Eq. 28) (—) and when nuclear polarization effects are included (Eq. 19 with Eqs. 23 and 29) (---). Note the large effect that k_q has on the ^{3}PI decay rate.

quinone depleted. A detailed treatment of spin-dynamics in Q-substituted RCs will be presented elsewhere.

NET NUCLEAR POLARIZATION PRODUCED BY CONTINUOUS ILLUMINATION

A net nuclear spin polarization can be produced by continuous illumination if the rates of nuclear spin relaxation are different in the different spin-polarized product states. The continuous illumination will produce a constant population in the ^{3}PI state. Since nuclear relaxation rates will be substantially different in the paramagnetic ^{3}PI and the diamagnetic ground state, the distribution of nuclear spin states in ^{3}PI will relax to an equilibrium distribution faster than the distribution of nuclear spins in the ground state. The result will be a net change in the total distribution of nuclear spin states in the sample, which will persist until nuclear relaxation occurs in the diamagnetic ground state. This mechanism is similar to the net CIDNP detected in cyclic reactions (Boxer, 1976; Closs, 1975).

To model the effect of nuclear spin relaxation, we make the approximation that the nuclear spins in the ^{3}PI state relax uniformly at rate $1/\tau_{^3PI}$, while the nuclear spins in the ground state relax at rate $1/\tau_{PI}$. This approximation is certainly not rigorously valid for ^{3}PI since the nuclei on paramagnetic ^{3}P will relax much more rapidly than those on diamagnetic I. It is the nonequilibrium distribution of $\mathbf{H_i}$ values that affects the results of an experiment: since $\mathbf{H_i}$ reflects the sum of the hyperfine fields due to all of the individual nuclear spins, the relaxation of the distribution of $\mathbf{H_i}$ towards an equilibrium distribution will likely be dominated by the fast-relaxing nuclei, making this approximation reasonable. The equations for the time dependence of the hyperfine field distributions in the ^{3}PI and PI states are then

$$\frac{d}{dt}R_{PI}(\mathbf{H_i}) = -k_e\phi(\mathbf{H_i})R_{PI}(\mathbf{H_i}) + k_{dec}(\mathbf{H_i})R_{^3PI}(\mathbf{H_i}) - \frac{R_{PI}(\mathbf{H_i}) - (1-\Gamma)R^0(\mathbf{H_i})}{\tau_{PI}} \quad (30)$$

$$\frac{d}{dt}R_{^3PI}(\mathbf{H_i}) = k_e\phi(\mathbf{H_i})R_{PI}(\mathbf{H_i}) - k_{dec}(\mathbf{H_i})R_{^3PI}(\mathbf{H_i}) - \frac{R_{^3PI}(\mathbf{H_i}) - \Gamma R^0(\mathbf{H_i})}{\tau_{^3PI}}, \quad (31)$$

where k_e is the rate of sample excitation and Γ is the total relative ^{3}PI population, given by

$$\Gamma = \int_{-\infty}^{\infty} R_{^3PI}(\mathbf{H_i})\, d\mathbf{H}_i. \quad (32)$$

For the steady-state distribution of hyperfine fields, Eqs. 30 and 31 are set equal to 0. The solution is then

$$\Gamma = \frac{\int_{-\infty}^{\infty}\gamma(\mathbf{H_i})k_e\phi(\mathbf{H_i})R^0(\mathbf{H_i})\,d\mathbf{H_i}}{\int_{-\infty}^{\infty}\gamma(\mathbf{H_i})[k_{dec}(\mathbf{H_i}) + k_e\phi(\mathbf{H_i})]R^0(\mathbf{H_i})\,d\mathbf{H_i}}, \quad (33)$$

$$R_{^3PI}(\mathbf{H_i}) = \left[\beta k_e\phi(\mathbf{H_i}) + \frac{\Gamma}{\tau_{^3PI}}\right]\gamma(\mathbf{H_i})R^0(\mathbf{H_i}), \quad (34)$$

and

$$R_{PI}(\mathbf{H_i}) = \left[\beta - \frac{\tau_{PI}}{\tau_{^3PI}}\left(\beta k_e\phi(\mathbf{H_i}) + \frac{\Gamma}{\tau_{^3PI}}\right)\gamma(\mathbf{H_i})\right]R^0(\mathbf{H_i}) \quad (35)$$

where

$$\beta = 1 - \Gamma\left[1 - \frac{\tau_{PI}}{\tau_{^3PI}}\right] \quad (36)$$

$$\gamma(\mathbf{H_i}) = \left[\frac{\tau_{PI}}{\tau_{^3PI}}k_e\phi(\mathbf{H_i}) + k_{dec}(\mathbf{H_i}) + \frac{1}{\tau_{^3PI}}\right]^{-1}. \quad (37)$$

After the illumination is turned off, the ^{3}PI state is modeled as decaying to the ground state with no nuclear relaxation. $R(\mathbf{H_i})$, the distribution of $\mathbf{H_i}$ values in the sample, is then

$$R(\mathbf{H_i}) = R_{PI}(\mathbf{H_i}) + R_{^3PI}(\mathbf{H_i}). \quad (38)$$

This expression can be integrated to give $R(\omega)$, the distribution of ω values in the sample. Fig. 5 gives typical plots of $R(\omega)$ for $\tau_{PI} = 1$ s, $\tau_{^3PI} = 1 \times 10^{-4}$ s, and $k_e = 1 \times 10^3$ s^{-1} (corresponding to ~0.5 W/cm^2 of 750-nm light) compared with equilibrium (no continuous illumination) distributions. The other components of $\mathbf{H_i}$ will also be polarized.

The nuclear spin polarization at 0 G is small, reflecting the fact that the pumping of the large ω states to smaller ω states is limited by the sparseness of possible small ω states. The polarization is surprisingly large at moderate field, becoming unimportant at very high fields as expected.

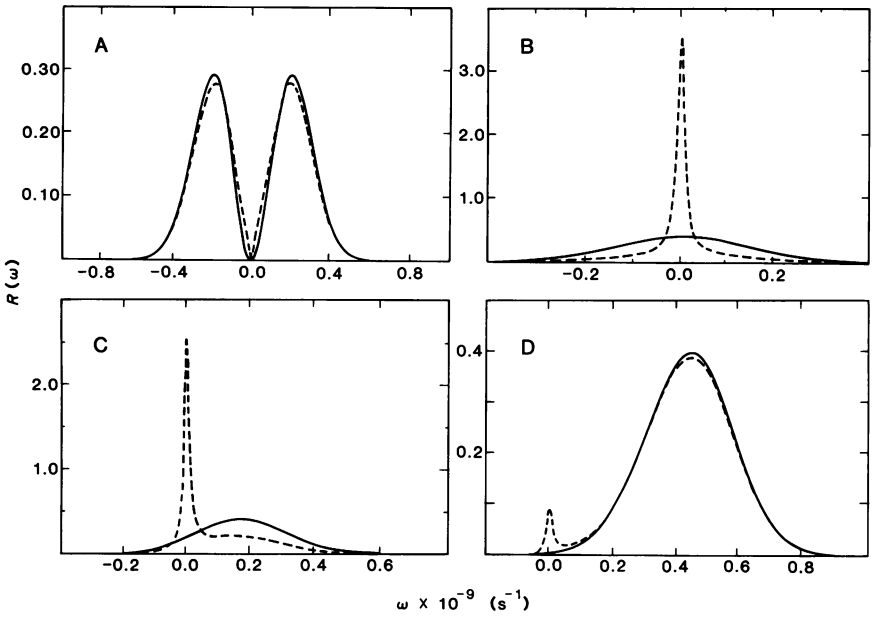

FIGURE 5 The effect of continuous illumination (~0.5 W/cm^2 at 750 nm, with τ_{PI} = 1 s, $\tau_{^3PI}$ = 1 × 10^{-4} s) on the distribution of ω, $R(\omega)$, at 0 G (*A*), 1 kG (*B*), 20 kG (*C*), and 50 kG (*D*). The resulting distribution of ω values in the sample (---) is compared with the equilibrium distribution [$R^0(\omega)$] (—). Note the difference in abcissa and ordinate scales.

A significant manifestation of this polarization is the variation in the steady-state population of ^{3}PI as the excitation intensity is increased (saturation curves). Fig. 6 gives computed saturation curves at 0 G and 1 kG. At both magnetic field strengths, the effect of nuclear spin polarization is significant, as increasing the excitation intensity increases the magnitude of the nuclear spin polarization, further reducing the triplet yield. The effect is especially dramatic at 1 kG.

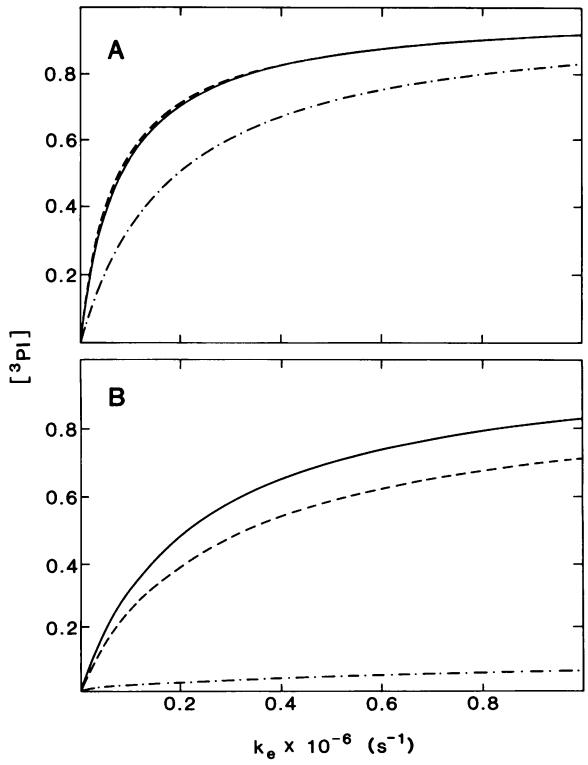

FIGURE 6 The effect of nuclear polarization on ^{3}PI saturation curves at 0 G (*A*) and 1 kG (*B*). Shown are calculated saturation curves for a sample with a single value of ω (—), an equilibrium distribution of ω values (----), and when nuclear relaxation (τ_{PI} = 1 s, $\tau_{^3PI}$ = 1 × 10^{-4} s) is included in the analysis (-·-·-). All of these models have the same triplet yield at k_e = 0.

This net spin polarization would also affect any measurement that depends upon the distribution of hyperfine fields in the sample. The effect of such polarization on $\Phi_{^3PI}$, k_{obs}, and k_{RP} at 1 kG are shown in Fig. 7. The polarization of the sample results in a lower triplet yield, and a slower ^{3}PI and radical-pair decay rate, for the reasons developed above.

This polarization may be produced whenever there is significant recycling of the sample through the radical-pair state during the ground state nuclear spin relaxation time. This polarization will persist until the nuclear spins in the ground state relax, which can be on the order of seconds at room temperature and considerably longer at low temperature.

CONCLUSION

Either of the two mechanisms discussed above for the production of nuclear spin polarization may be effective under certain circumstances. The sorting of nuclear spin states in the radical-pair state will be important whenever there is re-formation of the radical-pair state before the ^{3}PI state has a chance to decay, for instance, if the fraction of the sample that has decayed directly to the ground state is reexcited during this time. It is important to note that at room temperature there are intrinsic processes, such as the decay of ^{3}PI, that re-form the radical-pair state and will be sensitive to these nuclear polarization effects.

The net nuclear spin polarization produced by differential nuclear spin relaxation will be important when there is significant recycling of the RCs through the radical-pair state during the nuclear spin relaxation time of the ground

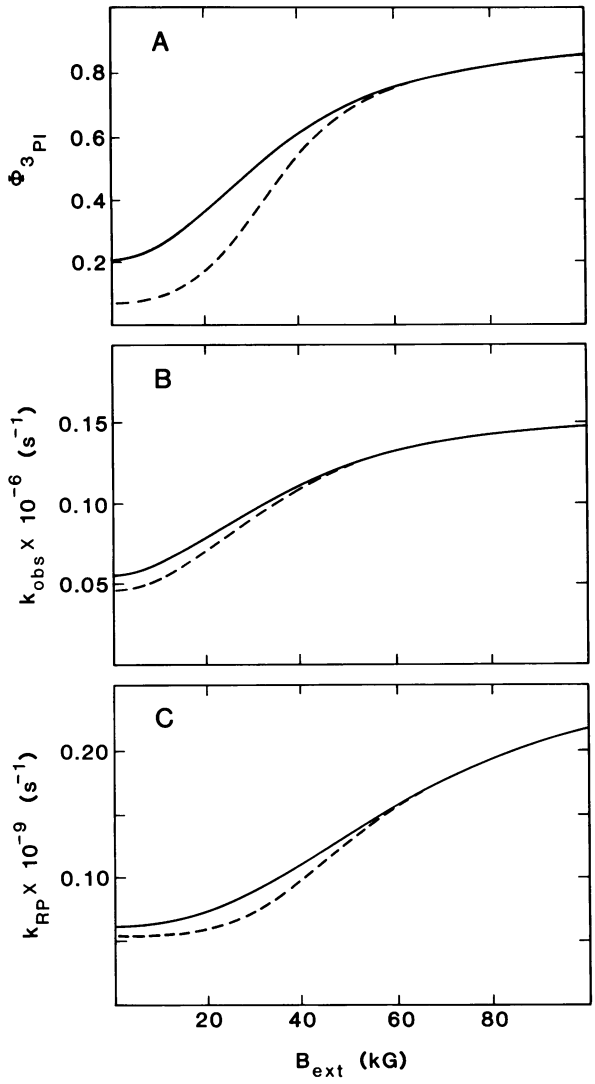

FIGURE 7 The effect of the nuclear polarization produced by continuous illumination (~0.5 W/cm^2 at 750 nm) on the ^{3}PI yield (*A*), k_{obs} (*B*), and k_{RP} (*C*), as a function of magnetic field. The calculated values for a polarized sample (----) are compared with those calculated for a sample at equilibrium (—).

state. This effect can be studied systematically, and may also cause large changes in many standard measurements that use intense continuous or high-repetition rate light sources or are performed at low temperatures. It should be noted that nuclear spin relaxation times at low temperatures in solids can be extremely long (seconds or longer). The kinetics and yield of any state whose formation or decay involves singlet–triplet mixing would be susceptible to these effects. This would include, besides those discussed here, fluorescence lifetimes and yields and quinone reduction yields (for substituted quinones with k_q small enough for electron spin evolution to occur).

Because nuclear spin polarization effects are sensitive to different properties of RCs than other magnetic field effects, our analysis suggests that experiments probing this effect may provide information about RC dynamics not obtainable from other methods. It will be especially interesting to measure the effects of radiofrequency (rf) fields resonant with nuclear spin transitions on any of these observables in a moderate magnetic field. Resonant rf will scramble the nuclear spin states, reducing the polarization. Thus, rf experiments would both confirm the presence of nuclear spin polarization and provide an approach to obtaining low resolution NMR spectra of the ground and ^{3}PI states. These experiments, as well as others, are currently in progress in this lab.

This work was supported in part by National Science Foundation Grants DMB-8352149 and DMB-8607789. R. A. Goldstein was a National Science Foundation Predoctoral Fellow.

Received for publication 10 September 1986.

REFERENCES

Boxer, S. G. 1976. Excited states, electron transfer reactions and dimers of chlorophyll derivatives and related model systems. Ph.D. Thesis. University of Chicago.

Boxer, S. G., C. E. D. Chidsey, and M. G. Roelofs. 1983. Magnetic field effects on reaction yields in the solid state: an example from photosynthetic reaction centers. *Annu. Rev. Phys. Chem.* 34:389–417.

Chidsey, C. E. D., L. Takiff, R. A. Goldstein, and S. G. Boxer. 1985. Effect of magnetic fields on the triplet state lifetime in photosynthetic reaction centers: evidence for thermal repopulation of the initial radical pair. *Proc. Natl. Acad. Sci. USA.* 82:6850–6854.

Closs, G. L. 1969. A mechanism explaining nuclear spin polarization in radical recombination reactions. *J. Am. Chem. Soc.* 91:4552–4554.

Closs, G. L. 1975. On the overhauser mechanism of chemically induced nuclear polarization as suggested by Adrian. *Chem. Phys. Lett.* 32:277–278.

Deisenhofer, J., O. Epp, K. Miki, R. Huber, and H. Michel. 1984. X-ray structure analysis of a membrane protein complex. Electron density map at 3Å resolution and a model of the chromophores of the photosynthetic reaction center from *Rhodopseudomonas viridis*. *J. Mol. Biol.* 180:385–398.

Goldstein, R. A., and S. G. Boxer. 1986. Effects of nuclear polarization on reaction dynamics in photosynthetic reaction centers. *Biophys. J.* 49:584a.

Gunner, M. R., D. E. Robertson, and P. L. Dutton. 1986. Kinetic studies on the reaction center protein from *Rhodopseudomonas sphaeroides:* the temperature and free energy dependence of electron transfer between various quinones in the Q_A site and the oxidized bacteriochlorophyll dimer. *J. Phys. Chem.* 90:3783–3795.

Haberkorn, R., and M. E. Michel-Beyerle. 1979. On the mechanism of magnetic field effects in bacterial photosynthesis. *Biophys. J.* 26:489–498.

Hoff, A. J. 1979. Applications of ESR in photosynthesis. *Phys. Rep.* 54:75–200.

Hoff, A. J. 1986. Magnetic interactions between photosynthetic reactants. *Photochem. Photobiol.* 43:727–745.

Kaptein, R., and L. J. Oosterhoff. 1969. Chemically induced dynamic nuclear polarization. *Chem. Phys. Lett.* 4:195–197.

Kaufmann, K. J., P. L. Dutton, T. L. Netzel, J. S. Leigh, and P. M. Rentzepis. 1975. Picosecond kinetics of events leading to reaction center bacteriochlorophyll oxidation. *Science (Wash. DC).* 188:1301–1304.

Kirmaier, C., D. Holten, R. J. Debus, G. Feher, and M. Y. Okamura. 1986. Primary photochemistry of iron-depleted and zinc-reconstituted reaction centers from *Rhodopseudomonas sphaeroides. Proc. Natl. Acad. Sci. USA.* 83:6407–6411.

Lersch, W., and M. E. Michel-Beyerle. 1983. Magnetic field effects on

the recombination of radical ions in reaction centers of photosynthetic bacteria. *Chem. Phys.* 78:115–126.

Martin, J.-L., J. Breton, A. J. Hoff, A. Migus, and A. Antonetti. 1986. Femtosecond spectroscopy of electron transfer in the reaction center of the photosynthetic bacterium *Rhodopseudomonas sphaeroides* R-26: direct electron transfer from the dimeric bacteriochlorophyll primary donor to the bacteriopheophytin acceptor with a time constant of 2.8 ± 0.2 psec. *Proc. Natl. Acad. Sci. USA.* 83:957–961.

Norris, J. R., M. K. Bowman, D. E. Budil, J. Tang, C. A. Wraight, and G. L. Closs. 1982. Magnetic characterization of the primary state of bacterial photosynthesis. *Proc. Natl. Acad. Sci. USA.* 79:5532–5536.

Ogrodnik, A., W. Lersch, M. E. Michel-Beyerle, J. Deisenhofer, and H. Michel. 1985. Spin dipolar interactions of radical pairs in photosynthetic reaction centers. *Springer Ser. Chem. Phys.* 42:198–206.

Okamura, M. Y., R. A. Isaacson, and G. Feher. 1975. Primary acceptor in bacterial photosynthesis: obligatory role of ubiquinone in photoactive reaction centers of *Rhodopseudomonas spheroides*. *Proc. Natl. Acad. Sci. USA.* 72:3491–3495.

Rockley, M. R., M. W. Windsor, R. J. Cogdell, and W. W. Parson. 1975. Picosecond detection of an intermediate in the photochemical reaction of bacterial photosynthesis. *Proc. Natl. Acad. Sci. USA.* 72:2251–2255.

Roelofs, M. G., C. E. D. Chidsey, and S. G. Boxer. 1982. Contributions of spin-spin interactions to the magnetic field dependence of the triplet quantum yield in photosynthetic reaction centers. *Chem. Phys. Lett.* 87:582–588.

Schulten, K., and P. G. Wolynes. 1978. Semiclassical description of electron spin motion in radicals including the effect of electron hopping. *J. Chem. Phys.* 68:3292–3297.

Shuvalov, V. A., and W. W. Parson. 1981. Energies and kinetics of radical pairs involving bacteriochlorophyll and bacteriopheophytin in bacterial reaction centers. *Proc. Natl. Acad. Sci. USA.* 78:957–961.

Werner, H., K. Schulten, and A. Weller. 1978. Electron transfer and spin exchange contributing to the magnetic field dependence of the primary photochemical reaction of bacterial photosynthesis. *Biochim. Biophys. Acta.* 502:255–268.